Physical Structure of Constitutional Isomers Influences Antiproliferation Activity of Thiosemicarbazone-Alkylthiocarbamate Copper Complexes

Kritika Bajaj,[a] Sarah A. Andres,[b] Dillon T. Hofsommer,[a] Aidan F. Greene,[a] Oleksandr Hietsoi,[c] Mark S. Mashuta,[a] Theresa Weis,[b] Levi J. Beverly,[b] Paula J. Bates,[b] Robert M. Buchanan,[a*] Craig A. Grapperhaus[a*]*

[a]Department of Chemistry, University of Louisville, Louisville, Kentucky 40292, United States. [b]Department of Medicine and Brown Cancer Center, University of Louisville, Louisville, Kentucky 40202, United States. [c]Department of Chemistry, Middle Tennessee State University, Murfreesboro, TN, 37132, United States.

Keywords: Copper, antiproliferation activity, thiosemicarbazone, alkythiocarbamate, N_2S_2 ligands, constitutional isomers

Abstract

A series of hybrid thiosemicarbazone-alkylthiocarbamate copper complexes with similar electronic environments but distinct physical structures have been prepared, characterized, and evaluated for antiproliferation activity. The complexes include the constitutional isomers (1-phenylpropane-1-imine-(O-ethylthiocarbamato)-2-one-(N-methylthiosemicarbazonato))copper(II) (CuL^1) and (1-phenylpropane-1-one-(N-methylthiosemicarbazonato)-2-imine-(O-ethylthiocarbamato))copper(II) (CuL^2) along with (1-propane-1-imine-(O-ethylthiocarbamato)-2-one-(N-methylthiosemicarbazonato))copper(II) (CuL^3). Complexes CuL^1 and CuL^2 differ in the positions of the pendent thiosemicarbazone (TSC) and alkylthiocarbamate (ATC) moieties on the 1-phenylpropane backbone. Complex CuL^3 employs a propane backbone with the TSC in the 2-position as in CuL^1. The isomer pair CuL^1 and CuL^2 have equivalent electronic environments with indistinguishable $Cu^{II/I}$ potentials ($E_{1/2}$ = -0.86 V vs. ferrocenium/ferrocene) and electron paramagnetic resonance (EPR) spectra ($g_{\|}$ = 2.26, $g_{\perp}$ = 2.08). The electronic structure of CuL^3 has a similar $E_{1/2}$ of -0.84 V and identical EPR parameters to CuL^{1-2}. Single crystal X-ray diffraction studies confirm a consistent donor environment with no substantial variation in the Cu-N or Cu-S bond distances and angles between the complexes. The antiproliferation activities of the CuL^{1-3} were evaluated against the lung adenocarcinoma cell line (A549) and nonmalignant lung fibroblast cell line (IMR-90) using the MTT assay. CuL^1 had the highest A549 activity ($^{A549}EC_{50}$ = 0.065 μM) and selectivity ($^{IMR\text{-}90}EC_{50}/^{A549}EC_{50}$ = 20). The constitutional isomer CuL^2 displayed decreased A549 activity (0.18 μM) and selectivity (10.6). The complex CuL^3 displayed activity (0.009 μM) similar to CuL^1 but with a lack of selectivity (1.0). Cellular copper loading determined by ICP-MS were consistent with the activity and selectivity trends. The complexes CuL^{1-3} did not induce reactive oxygen species (ROS) generation.

Introduction

The development and evaluation of copper complexes for diagnostic and therapeutic applications has attracted significant attention due to their promising efficacy and lower potential toxicity than other metals such as platinum.[1] Copper is an essential metal with Cu(II) and Cu(I) oxidation states common in biological systems. It is found in various redox active enzymes including oxygenases and oxidases such as cytochrome C oxidase and Cu/Zn superoxide dismutase.[2,3] It also serves as a metal signaling agent in response to external stimuli leading to copper-dependent cell growth and proliferation (cuprolasia) or cell death (cuproptosis).[4-6] The range of potential applications for small molecule Cu complexes is exemplified by the evaluation of Cu(BTSC) (BTSC = bis(thiosemicarbazone) complexes) for the treatment of neurodegenerative diseases,[7,8] imaging of hypoxia and oxidative stress,[9-11] and a wide range of pharmacological activities including antitumor,[12] antiviral,[13] antibacterial,[14] and antifungal properties.[15] Cu(BTSCs) are neutral Cu(N_2S_2) complexes with $Cu^{II/I}$ reduction potentials that can be tuned by variation of the ligand backbone (R^1, R^2) and pendent amine (R^3, R^4) substituents (Figure 1).[16,17] Recently, we developed bis(alkylthiocarbamate) (BATC) and hybrid thiosemicarbazone-alkylthiocarbamate (TSTC) N_2S_2 ligand systems (Figure 1) to introduce additional variability of physical and electronic structure.[18,19]

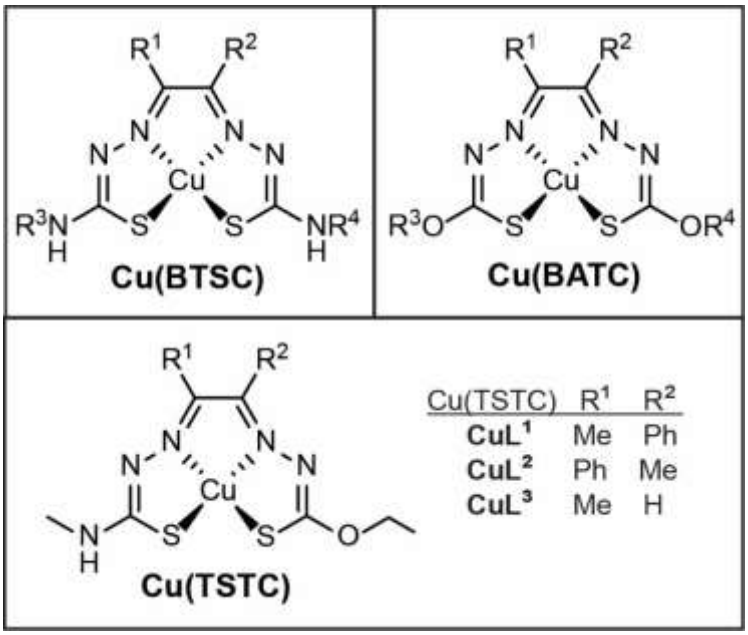

Figure 1. Structures of copper BTSC, TSTC, and BATC complexes.

The N_2S_2 copper(II) complexes in Figure 1 are neutral and rigidly planar making them suitable for passive or active cellular uptake.[16,17] It is widely accepted that the ligand acts as an ionophore[11,20] to facilitate cellular uptake of the Cu(II) complex, which may be reduced to Cu(I) by cellular reductants, such as NADH or glutathione.[21] The lowered oxidation state decreases the binding affinity of the ligand, enabling transfer or release of Cu^{I}, which is retained in the cell.[22] The activity of the copper complexes depends on both the inherent $Cu^{II/I}$ reduction potential, which is influenced by the coordination environment, and the relative level of intracellular redox agents (i.e. the redox status of the cell).[9] For example, the structurally similar CuGTSM ($R^{1,2}$ = H, $R^{3,4}$ = Me) and CuATSM ($R^{1\text{-}4}$ =Me) complexes display drastically different mechanisms of action due to differences in their electronic structures.[16,23] This may explain why we[19] and others[16] have seen that CuGTSM has strong antiproliferative effects on both cancer cells and non-cancer cells (i.e., high potency but low cancer selectivity), whereas CuATSM has moderate selectivity and modest potency. In addition to reduction potentials, other chemical and physical factors impact biological

activity. For example, lipophilicity influences activity and cellular uptake,[14] although highly lipophilic complexes can be trapped in the cell membrane, hindering their interaction with the intracellular reductants.[24,25]

In the current manuscript, we report the influence of physical structure on the anti-proliferation activity and selectivity of Cu(TSTC) complexes. In previous studies, we reported the synthesis, characterization and biological activity of Cu(TSTC)[19] and Cu(BATC)[18,26] complexes for comparison with Cu(BSTCs). Those studies employed a series of complexes with varied electronic structures that revealed differences in antiproliferation activity and selectivity that do not strictly correlate with changes in the $Cu^{II/I}$ potential. Interestingly, the hybrid Cu(TSTC) complexes have both higher antiproliferation activity against the A549 lung adenocarcinoma cell line (EC_{50} < 100 nM) and higher selectivity for A549 versus the nonmalignant IMR-90 lung fibroblast cell line (selectivity = $^{IMR\text{-}90}EC_{50}/^{A549}EC_{50} \geq 20$) than their Cu(BTSC) and Cu(BATC) congeners. In order to systematically evaluate the effect of changes in physical structure, we herein report the synthesis and evaluation of a series of Cu(TSTC) complexes with nearly equivalent electronic environments but different physical structures. Complexes CuL^1 and CuL^2 are constitutional isomers with the same chemical formula but different connectivity and CuL^3 is a derivative with R^1 = H, which results in a similar electronic environment as $CuL^{1\text{-}2}$. The results clearly show that the relative arrangement of the thiosemicarbazone (TSC) and alkylthiocarbamate (ATC) functional groups with respect to the backbone substituents substantially effects A549 antiproliferation activity and IMR90/A549 selectivity.

Experimental

Materials and Methods

All reagents were commercially available and used as received unless otherwise noted. Hydrazinecarbothioic acid *O*-ethyl ester[27] and the CuL^1 complex[19] were prepared by following literature methods. The ligand precursors 1-phenyl-1-propanone-2-(ethylthiocarbamate) and 1-propanone-2-(4-N-methyl-3-thiosemicarbazone) were prepared by modification of a related literature procedure[28] as detailed with characterization (Figures S1 – S6) in the supporting information. Solvents were dried and purified using an MBraun solvent purification system. The complexes in this study are air and water stable as solids and were handled on the benchtop with no required protection from the atmosphere.

Synthetic Procedures

CuL^2. 1-phenyl-1-propanone-2-(ethylthiocarbamate) (0.5 g, 1.99 mmol) and 4-*N*-methyl-3-thiosemicarbazide (0.21 g, 1.99 mmol) were suspended in ethanol (25 mL) and the reaction solution was stirred at room temperature for 48 h. Crude H_2L^2 (0.45 g) was obtained as a white solid by filtration, washed with ethanol, and used without further purification. A portion of the white solid (0.10 g) was suspended in methanol (10 mL) and copper(II) acetate monohydrate (0.059 g, 0.30 mmol) was added producing a red-brown precipitate. The reaction mixture was refluxed for 4 h. After cooling, the red-brown solid was filtered and washed with methanol. The complex was crystallized by slow evaporation of an acetonitrile solution. (Yield = 0.55 g, 46%). IR (cm^{-1}): 3328 and 1542 (NH), 2984 and 1438 (CH), 1383 and 1223 (CN), 1012 (CO), 975 (CS), 870 (CuS), 759 (CuN). UV−Vis spectrum in acetonitrile (nm) (M^{-1} cm^{-1}): 278 sh (23,000), 314 (19,000), 358 sh (12,000), 489 (5,300), 542 sh (2,700). Elemental analysis for $C_{14}H_{17}N_5OS_2Cu$: C, 42.14; H, 4.29; N, 17.55. Found: C, 41.99; H, 4.24; N, 17.02. Mass spectrum for $Cu(HL^2)^+$: 399.0243. Found: 399.0245.

CuL^3. A catalytic amount of hydrochloric acid (6 drops) and hydrazinecarbothioic acid O-ethyl ester (0.37 g, 3.14 mmol) were added to an ethanol (25 mL) suspension of 1-propanone-2-(4-*N*-methyl-3-thiosemicarbazone) (0.5 g, 3.14 mmol), and the reaction solution was stirred at room temperature overnight. Crude H_2L^3 (0.54 g) was obtained as a white solid by filtration, washed with ethanol, and used without further purification. A portion of the white solid (0.10 g) was suspended in methanol (10 mL) and copper(II) acetate monohydrate (0.076 g, 0.38 mmol) was added giving a red-brown precipitate. The reaction mixture was refluxed for 4 h. Upon cooling the red-brown solid was filtered and washed with methanol. The product was recrystallized from a 1.5:1 mixture of ethanol and acetonitrile (Yield = 0.79 g, 64%). IR (cm^{-1}): 3231 and 1547 (NH), 2950 and 1458 (CH), 1365 and 1219 (CN), 1026 (CO), 925 (CS), 890 (CuS), 805 (CuN). UV−Vis spectrum in acetonitrile (nm) (M^{-1} cm^{-1}): 251 (10,000), 317 (12,000), 358 sh (6,900), 493 (4,100), 547 sh (2,100). Elemental analysis for $C_8H_{13}N_5OS_2Cu$: C, 29.76; H, 4.06; N, 21.69. Found: C, 29.60; H, 3.76; N, 21.33. Mass spectrum for $Cu(HL^3)^+$: 322.9930. Found: 322.9932.

Physical methods

Elemental analyses were performed by Micro-analysis, Inc. (Wilmington, DE). The electronic spectra were collected on acetonitrile solutions of the Cu complexes using 1 mm quartz cuvettes and Agilent 8453 diode array spectrometer. The vibrational spectra were obtained as powders on a Nicolet 360 FT-IR with a Smart iTR attachment. The NMR spectra were recorded on a Varian 700 MHz spectrometer at room temperature. Mass spectra were collected by the Mass Spectrometry Facility at Indiana University (+ESI-MS). All EPR spectra were collected by the Ohio Advanced EPR Laboratory at Miami University on frozen solutions in DMF at 77 K.

Electrochemical measurements

All electrochemical data were recorded using a Gamry 1000 Potentiostat/Galvanostat/ZRA. The complexes were dissolved in acetonitrile (0.3 mM) under argon in a Gamry three electrode cell. Tetrabutylammonium hexafluorophosphate (0.1 M) was used as a supporting electrolyte. Glassy carbon was used as a working electrode, platinum as a counter electrode, and a silver wire immersed in a glass tube with a Teflon frit containing 0.1 M tetrabutylammonium hexafluorophosphate was used as quasi reference electrode. A small amount of ferrocene was added as an internal standard and all potentials are referenced versus ferrocenium/ferrocene (Fc^+/Fc^0).

Crystallographic Studies

Crystals of CuL^2 suitable for X-ray analysis were grown by slow evaporation of an acetonitrile solution and mounted on a glass fiber for collection of X-ray data on an Agilent Technologies/Oxford Diffraction Gemini CCD diffractometer. X-ray structural analysis was performed on a 0.50 x 0.11 x 0.02 mm^3 orange plate using a 500 frame, twenty second frame ω-scan data collection strategy at 102 K to a $2\theta_{max}$ = 56.56°. CuL^2 crystallizes in the monoclinic space group C_2/c with unit cell parameters: a = 28.0911(9) Å, b = 6.8829(2) Å, c = 16.8291(6) Å, β = 94.752(3)°, V = 3242.70(19) $Å^3$, D_{calc} = 1.635 Mg/m^3, Z = 8 to produce raw hkl data that were then corrected for absorption (transmission min./max. = 0.773 /1.000; μ = 1.615 mm^{-1}). The structure was solved by Patterson methods using SHELXS.[29] All non-hydrogen atoms were refined with anisotropic atomic displacement parameters. Imine NH, methylene and phenyl hydrogen atoms were located by difference maps and refined isotropically. Methyl hydrogen atoms were placed in their geometrically generated positions and refined as a riding model and these atoms were assigned U(H) = 1.5 Ueq of the carbon atom they are attached to respectively. For all 20,920

unique reflections (R(int) 0.031) the final anisotropic full matrix least-squares refinement on F^2 for 252 variables converged at R1 = 0.038 and wR2 = 0.079 with a GOF of 1.03.

Crystals of CuL^3 suitable for X-ray analysis were grown by slow evaporation of a 1.5:1 acetonitrile/acetone solution. X-ray structural analysis for CuL^3 was performed on a 0.41 x 0.13 x 0.08 mm^3 purple prism using an identical data acquisition strategy described above for CuL^2 at 102 K to a $2\theta_{max}$ = 62.54°. CuL^3 crystallizes in the monoclinic space group $P2_1/c$ with unit cell parameters: a = 14.9123(4) Å, b = 20.8951(12) Å, c = 7.9465(4)Å, β = 92.760(3)°, V = 2473.2(2) $Å^3$, Z = 4 and D_{calc} = 1.734 Mg/m^3. Raw independent data were corrected for absorption (transmission min./max. = 0.847 /1.000; μ = 2.094 mm^{-1}). The structure was solved by Patterson methods using SHELXTL. All non-hydrogen atoms were refined with anisotropic atomic displacement parameters. All hydrogen atoms were located by difference maps and refined isotropically. For all 8,066 unique reflections (R(int) 0.044) the final anisotropic full matrix least-squares refinement on F^2 for 411variables converged at R1 = 0.045 and wR2 = 0.066 with a GOF of 1.04.

Cell studies

A549 and IMR-90 cells were purchased from the American Type Culture Collection (ATCC, Manassas, VA). Cells were grown in the appropriate medium supplemented with 10% fetal bovine serum (FBS, Life Technologies, Grand Island, NY), 62.5 μg/mL penicillin and 100 μg/mL streptomycin (Life Technologies) in a humidified incubator at 37 ºC with 5% CO_2. The growth media were as follows: Dulbecco's modified Eagle's medium (DMEM, Life Technologies) for A549 cells, and Eagle's minimal essential medium (EMEM) with Eagle's balanced salt solution (EBSS), 2 mM L-glutamine, 1500 mg/L sodium bicarbonate (Lonza, Walkersville, MD), supplemented with 1 mM sodium pyruvate (Life Technologies) and non-essential amino acids

(Life Technologies) for IMR-90 cells. For treatment, metal complexes were dissolved first in 100% DMSO and then diluted in aqueous medium. The final concentration of DMSO used in the assays was always less than 0.5% v/v.

Antiproliferative activity of the metal complexes was evaluated using a previously published 3-(4,5-dimethylthiazol-2-yl)-2,5-diphenyltetrazolium bromide (MTT) assay protocol.[19,30] Cells were seeded in quadruplicate wells in 96-well plates and allowed to adhere overnight. To account for intrinsic differences in growth rates, cells were plated at the following densities to achieve comparable MTT absorbance values (OD570 between 0.5 and 1) for untreated cells: A549, 1000 cells/well; IMR-90, 5000 cells/well. After 72 h of treatment with the various complexes or vehicle control, MTT (Sigma/Millipore Sigma, St. Louis, MO) was added for 4 h prior to cell lysis. All readings were normalized to the vehicle treatment. EC_{50} values were determined from ≥3 independent replicates with each experiment having 4 technical replicates.

Copper uptake using ICP-MS

A549 and IMR-90 cells were plated on 10 cm dishes at a density of 1 X 10^6 cells in a volume of 10 mL using the same growth media as in the cell studies noted above. Both cell lines were placed in a humidified incubator at 37 ºC with 5% CO_2 and left in an incubator overnight to allow cells to adhere. After the incubation, the cells were treated with the copper complex at a final concentration of 500 nM for 4 hours. After 4 hours of treatment, the cells were trypsinized and collected by centrifugation using standard methods. The cells were suspended in 1 mL 0.9% NaCl solution for a final wash, transferred to 1.5 mL tubes, and centrifuged at 100Xg for 5 min at 4 °C to obtain cell pellets. The pellets were stored on dry ice for transport. Further acid digestion and Cu analysis was conducted by the Centre of Applied Isotope Studies, University of Georgia. Cu/Zn loading data were determined from 2 technical replicates.

Results and Discussion

Synthesis and Characterization

A series of hybrid thiosemicarbazone-alkylthiocarbamate copper complexes (Figure 1) were synthesized and characterized. The complexes CuL^1 and CuL^2 are constitutional isomers that differ in the positions of the pendent TSC and ATC moieties on the 1-phenylpropane backbone. In CuL^1 the ATC is in the 1-position on the same side of the molecule as the backbone phenyl group and the TSC is in the 2-position on the same side as the backbone methyl. For CuL^2, the TSC is in the 1-position and the ATC is in the 2-position. Complex CuL^3 employs a propane backbone with the ATC in the 1-position and the TSC in the 2-position as in CuL^1. The copper complexes were prepared by refluxing equimolar quantities of ligand and copper(II) acetate monohydrate in methanol for 4 h, as described previously for CuL^1.[19] Complexes were obtained in moderate to high yields as air and water stable red-brown solids. The absence of hydrazine N–H stretches near 3200 cm^{-1} and shifts in the Cu–N and Cu–S stretching frequencies to lower energies in the FT-IR spectra (Figures S7 – S9) confirms complexation of the ligand to Cu(II) in the deprotonated, anionic form $(L^{1\text{-}3})^{2-}$.

A comparison of selected metric parameters for $CuL^{1\text{-}3}$ is provided in Table 1. The structure of CuL^1 was previously reported.[19] Crystal structure data and structure refinement details for CuL^2 and CuL^3 are provided in Table S1. For CuL^1 and CuL^2, metric parameters are for one of the two equivalents found within the asymmetric unit. The second equivalent is statistically equivalent and there are weak interactions between the two equivalents through long (> 2.7 Å) Cu–S apical interactions. ORTEP representations of $CuL^{1\text{-}3}$ as mononuclear square planar complexes are provided in Figure 2. The Cu atoms for the three complexes sit in a square planar N_2S_2 coordination environment with alternating single and double bonds within the ligand consistent with extended

conjugation. Excluding the phenyl ring, CuL^2 is rigidly planar with an average deviation of 0.041 Å for non-hydrogen atoms from the mean plane. The phenyl ring of CuL^2 is rotated with respect to the metal-ligand plane with a N1–C1–C4–C5 torsion angle of -113.92(19)° similar in magnitude to the corresponding torsion angle of 121.4(2)° in CuL^1. For CuL^3, the Cu sits 0.1340(2) Å above the mean S1 S2 N1 N3 donor plane due to the long-range apical interaction in the solid-state, which is similar to the corresponding deviation of 0.1654(2) Å in CuL^1. For CuL^{1-3}, there is no substantial variation between the complexes in the Cu–N or Cu–S bond distances, which range from 1.9626(14) to 1.9831(15) Å and 2.2239(5) to 2.2871(5) Å, respectively. Likewise, the bond distances within the ligand frameworks are statistically equivalent. Overall, the structural core is conserved across the series with the only significant differences in the physical structure associated with constitutional isomers (CuL^1/CuL^2) or substitution of H for Ph (CuL^1/CuL^3).

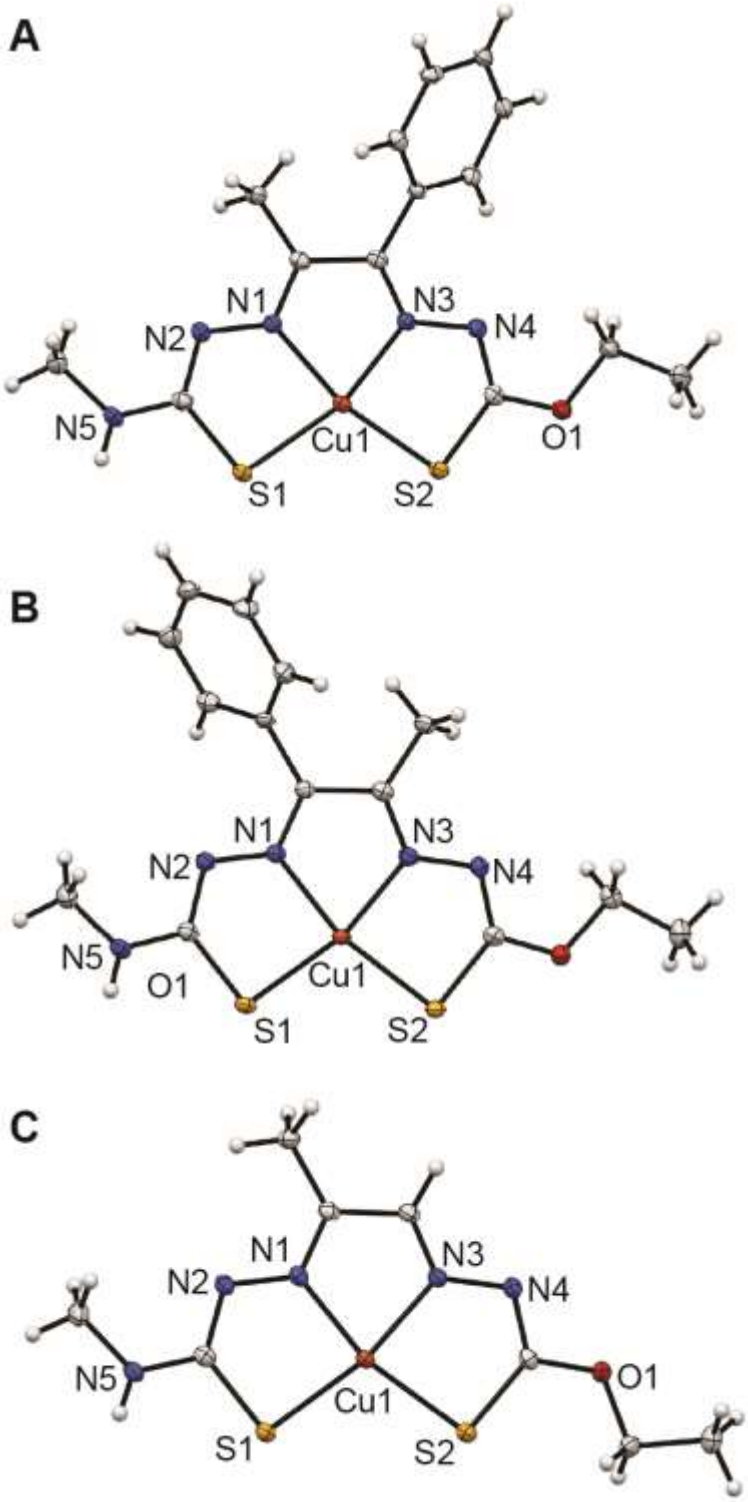

Figure 2. ORTEP representations with thermal ellipsoids displayed at 50% probability level for A) CuL^1 (from reference [19]), B) CuL^2, and C) CuL^3.

Table 1: Selected bond distances (Å) and angles (°) for CuL^{1-3}.[a]

	CuL^1	CuL^2	CuL^3
Bond distances			
Cu1-N1	1.9755(15)	1.9831(15)	1.9638(14)
Cu1-N3	1.9591(13)	1.9509(15)	1.9626(14)
Cu1-S1	2.2725(5)	2.2239(5)	2.2606(5)
Cu1-S2	2.2871(5)	2.2651(5)	2.2548(5)
N1-N2	1.3611(19)	1.368(2)	1.3586(19)
N1-C1	1.298(2)	1.300(2)	1.306(2)
N2-C[b]	1.319(2)	1.330(2)	1.333(2)
N3-N4	1.366(2)	1.380(2)	1.3754(19)
N3-C2	1.294(2)	1.292(2)	1.289(2)
N4-C[c]	1.304(2)	1.304(2)	1.316(2)
S1-C[b]	1.7584(19)	1.7492(18)	1.7694(17)
S2-C[c]	1.7377(16)	1.7438(19)	1.7342(17)
Bond angles			
N1-Cu1-N3	79.68(6)	80.16(6)	80.77(6)
N1-Cu1-S1	83.31(4)	85.19(5)	85.62(4)
N3-Cu1-S2	84.49(5)	85.21(5)	84.54(4)
S1-Cu1-S2	111.36(2)	109.430(18)	108.211(17)
sum of four angles	358.85(9)	359.99(9)	359.14(8)

a) Data for CuL^1 from reference 19. b) C = C10 for CuL^{1-2} and C4 for CuL^3. c) C = C11 for CuL^{1-2} and C5 for CuL^3.

The summary of the electronic properties of CuL^{1-3} provided in Table 2 shows a high degree of similarity among the complexes. The electronic spectra of CuL^2 in acetonitrile (Figures S10 – S12) displays a metal-to-ligand charge transfer band at 489 nm with a shoulder at 542 nm and an ensemble of more intense peaks below 358 nm that is essentially indistinguishable from the spectra of its constitutional isomer CuL^1. The data indicates that changes in the relative position of the backbone substituent with respect to the pendent groups do not substantially affect the overall electronic structure. Notably, the electronic spectrum of CuL^3 displays a metal-to-ligand charge transfer band at 493 nm with a shoulder at 547 nm and peaks below 358 nm analogous to CuL^{1-2} suggesting that the backbone H in CuL^3 is electronically similar to the Ph in CuL^{1-2}. This is consistent with the observations in the solid state that the Ph of CuL^{1-2} is tilted with respect

$Cu(N_2S_2)$ plane ligand core and not in conjugation with the TSTC π-system. The similarity of the electronic structure is further demonstrated by the EPR spectra, recorded in frozen DMF solution (Figures S16 – S18). Axial spectra consistent with Cu(II) ions in a square planar coordination environment is observed with identical $g_{\parallel} = 2.26$ and $g_{\perp} = 2.08$ ($g_{avg} = 2.14$) values for CuL^1 and $CuL^{2.}$ and $g_{\parallel} = 2.25$ and $g_{\perp} = 2.08$ ($g_{avg} = 2.14$) for CuL^3. Overall, the spectroscopic results indicate the electronic structure is conserved across the CuL^{1-3} series.

The electronic environment at the copper center was also probed by cyclic voltammetry. In acetonitrile, each of the CuL^{1-3} complexes display a single, reversible reduction assigned to the $Cu^{II/I}$ couple (Figure 3) and a single, reversible oxidation (Figure S19). The $Cu^{II/I}$ potentials for the constitutional isomers CuL^1 and CuL^2 are indistinguishable with a value of -0.86 V (vs. Fc^+/Fc) for each complex. For CuL^3, substitution of H for Ph in the ligand backbone results in a small anodic shift to -0.84 V. Notably, an analog of $CuL^{1,3}$ with Me in place of Ph/H in the backbone displays a $Cu^{II/I}$ potential of -0.93 V,[19] which is shifted cathodically by 90 mV relative to CuL^3 due to increased electron donation by the Me group into the conjugated ligand system. The oxidation potential for all three complexes is observed at +0.44 V. These results highlight the similar donor ability of the Ph in $CuL^{1,2}$ with the H in CuL^3 and the consistency of the electronic structure for CuL^{1-3}.

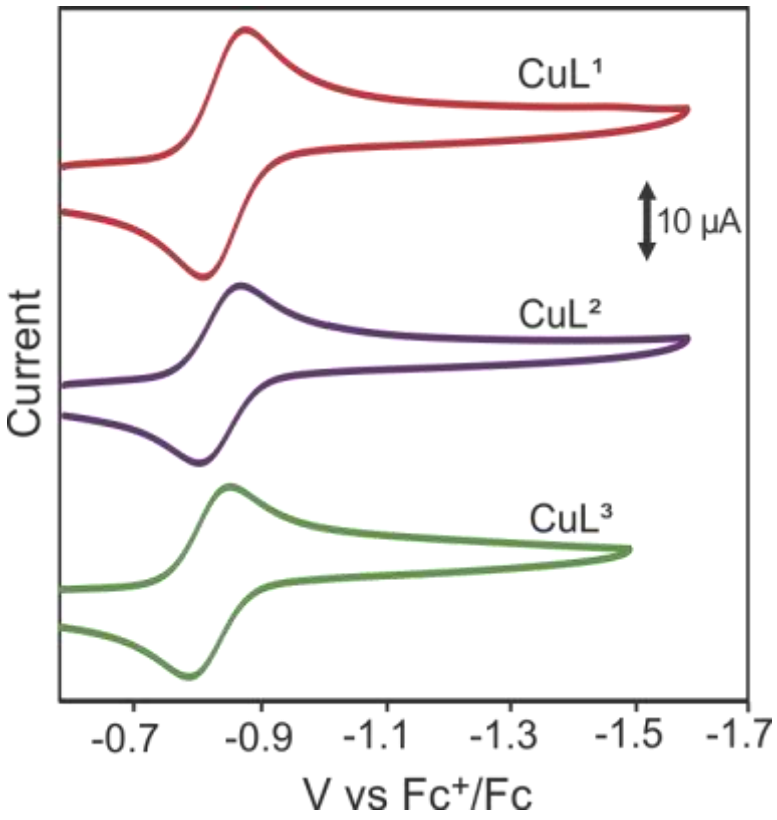

Figure 3. Cyclic voltammograms in acetonitrile with 0.1 M NBu_4PF_6 as supporting electrolyte at a scan rate of 200 mV s^{-1} for 0.3 mM CuL^1 (red), CuL^2 (purple), CuL^3 (green).

Table 2: Comparison of electronic properties of **CuL^{1-3}**.

Complex	$Cu^{II/I}$ Potential[a]	Electronic Spectra[a,c]		EPR[d]	
	$E_{1/2}$[b] (V)	λ_{max} (nm)	(ε) (M^{-1} cm^{-1})	$g_{\parallel}$, $g_{\perp}$ ($g_{avg.}$)	$A_{\parallel}$, $A_{\perp}$ (10^{-4} cm^{-1})
CuL^1	-0.86	263(sh) 310 358(sh) 490 547(sh)	26,000 27,000 16,000 6,500 3,500	2.26, 2.08 (2.14)	495, 70
CuL^2	-0.86	278(sh) 314 358(sh)	23,000 19,000 12,000	2.26, 2.08 (2.14)	500, 60

		489	5,300		
		542(sh)	2,700		
CuL^3	-0.84	251	10,000	2.25, 2.08	500, 60
		317	12,000	(2.14)	
		358(sh)	6,900		
		493	4,100		
		547(sh)	2,100		

a) $E_{1/2}$ and electronic spectral data for CuL^1 from reference 19. b) Potentials versus Fc^+/Fc in acetonitrile. c) Data collected in acetonitrile at room temperature. d) Data collected in frozen DMF at 77 K .

Antiproliferation Activity and Cu Uptake

The antiproliferation activities of CuL^{1-3} were screened against lung adenocarcinoma (A549) and nonmalignant lung fibroblast (IMR-90) cell lines using an MTT assay to determine the half maximal effective concentration (EC_{50}) for each complex (Figure 4). Selectivity is defined as the ratio of EC_{50} values for IMR-90/A549, with higher selectivity values indicative of enhanced activity against cancerous A549 cells relative to nonmalignant IMR-90 cells. The data summarized in Table 3 show that CuL^1 and CuL^2 exhibit similar activity against IMR-90 EC_{50} values of 1.3 and 1.9 μM, respectively, but CuL^1 is three times more active against A549 (0.065 μM) than CuL^2 (0.18 μM). The statistically different activity and selectivity of the constitutional isomers must arise from the change in the relative position of the backbone Ph substituent, as the complexes are electronically equivalent. Interestingly, substitution of the Ph group with H leads to an enhancement of activity for CuL^3 against both A549 (0.009 μM) and IMR-90 (0.009 μM) and a complete loss of selectivity. The activity and selectivity of CuL^3 is comparable to CuGTSM, which also contains H substituents in the ligand backbone. As the $E_{1/2}$ of CuL^3 and CuGTSM differ by 109 mV, the high activity/poor selectivity is attributed to the backbone H substituent. The similar electronic environment of CuL^3 with $CuL^{1,2}$ strongly suggests this is associated with a change in

the physical structure. All the copper complexes are 60 to 1000 times more potent against A549 than cisplatin with similar or much improved selectivity relative to IMR-90.

Cellular copper loading by A549 and IMR-90 cells after treatment with CuL^{1-3} or CuGTSM was quantified by ICP-MS (Table 3). In all cases, copper treatment increased Cu loading in A549 cells to a greater amount than in IMR-90 cells. Copper loading in A549 cells follows the same trend as antiproliferation activity with CuL^3 > CuGTSM > CuL^1 > CuL^2. The data for IMR-90 shows the highest Cu loading for CuGTSM followed by CuL^3, CuL^2, and CuL^1, which is also consistent with the observed antiproliferation activity with this cell line. As an internal control, cellular zinc loading was also measured. In all cases, treatment with the copper complexes had little to no effect on Zn loading. Overall, Cu loading correlates with antiproliferation activity and selectivity. These results clearly show that changes in the physical structure of the complex significantly influence cellular uptake and retention even in cases where electronic structure are similar.

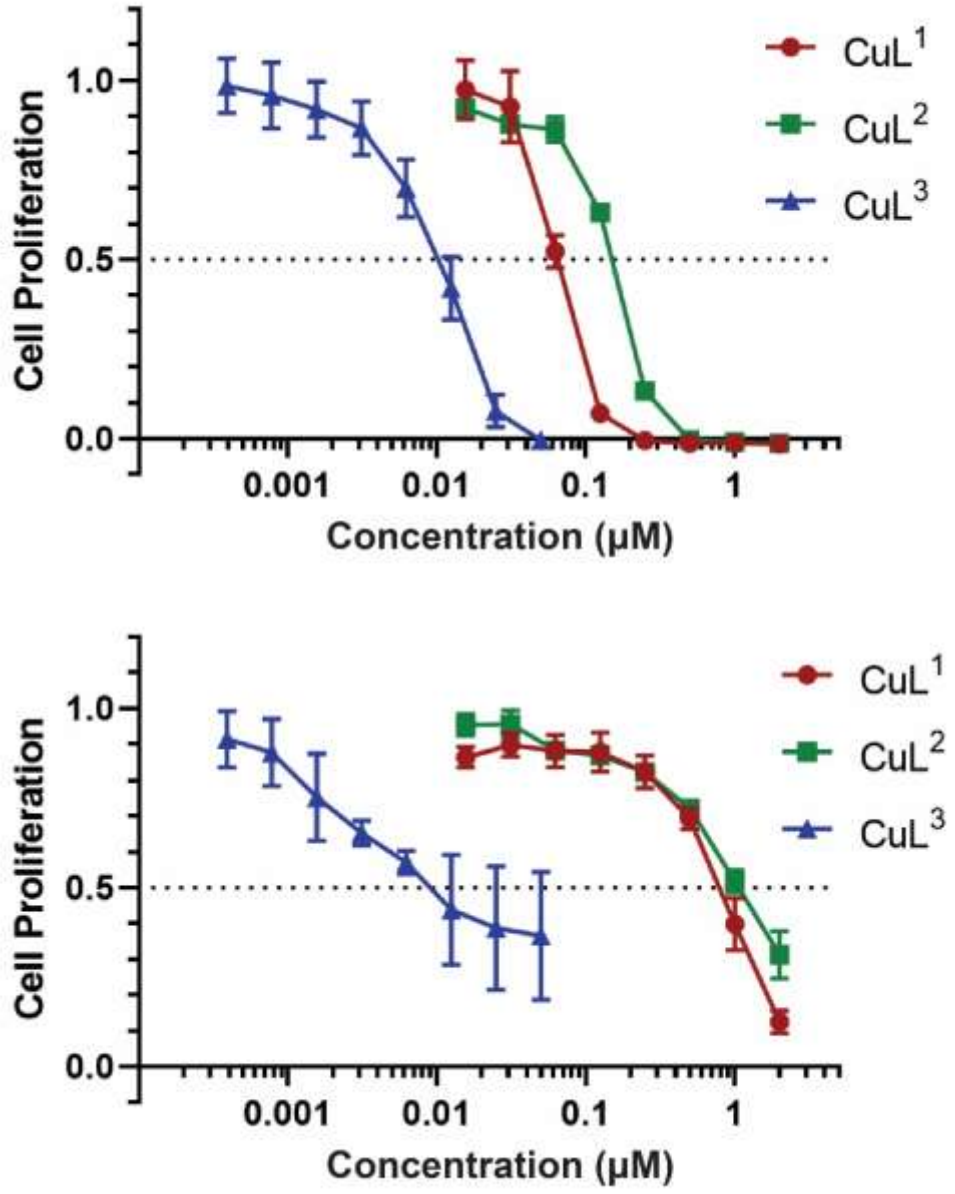

Figure 4. Cell proliferation results for A) A549 and B) IMR-90 cell lines treated with CuL^{1-3}. The dashed lines represent 50% cell proliferation (EC_{50}).

Table 3: Reduction potentials, EC_{50} (μM) values, and Cu/Zn loading for **CuL^{1-3}**, CuGTSM, cisplatin.[a]

Complex	$E_{1/2}$[b] (V)	$^{A549}EC_{50}$ (μM)	$^{IMR\text{-}90}EC_{50}$ (μM)	Selectivity[c]	Cu loading A549/IMR-90 (μg/g)	Zn loading A549/IMR-90 (μg/g)
CuL^1	-0.856	0.065	1.3	20	8.46/0.24	4.95/0.94
CuL^2	-0.863	0.180	1.9	10.6	4.24/0.40	4.25/0.92
CuL^3	-0.841	0.009	0.009	1.0	12.97/1.00	4.16/0.53
CuGTSM	-0.950	0.020	0.015	0.75	8.89/1.52	4.10/0.83
cisplatin		10.9	13.9	1.3	N.A.	N.A.
Vehicle (DMSO)	-				0.10/0.02	4.07/0.99

a) EC_{50} values were determined from ≥3 independent replicates with each experiment having 4 technical replicates. Cu/Zn loading data were determined from 2 technical replicates. b) $Cu^{II/I}$ potential versus Fc^+/Fc in acetonitrile. c) Selectivity = $^{IMR\text{-}90}EC_{50}/^{A549}EC_{50}$.

Comments and Conclusions

The anti-proliferation activity and selectivity of the Cu(TSTC) complexes CuL^{1-3} have been shown to be dependent on both the physical and electronic structure of the complex with improved selectivity for the constitutional isomers CuL^{1-2} relative to CuL^3 and the Cu(BTSC) complex CuGTSM. Structure–activity relationships of various Cu(BTSC) complexes have been evaluated in prior studies and their mechanisms of action are dependent on their physicochemical properties. For example, more lipophilic complexes are trapped in the cellular membrane making them more difficult to reduce and release Cu ions intracellularly[25] leading to lower activity.[31,32] As mentioned earlier, modulation of the $Cu^{II/I}$ reduction potentials by changing the backbone substituents and pendent groups influences both complex electronic properties and their potential applications. As noted above, CuGTSM, and CuATSM display drastically different mechanisms of action in relation to differences in their electronic structures.[16,23] The more cathodic reduction potential of

CuATSM compared to CuGTSM leads to greater resistance to intracellular reduction and dissociation of Cu(I) for CuATSM. This observation was further supported using a metal responsive element (MRE)-luciferase construct from transfected neuroblastoma SH-SY5Y cells, which responded with an increase in luminescence as bioavailable Cu levels increased.[23] When CuATSM and CuGTSM are added to MRE-luciferase-transfected cells, only CuGTSM demonstrated significant changes in bioluminescence, which correlated with greater intracellular release of bioavailable Cu for CuGTSM.[23] CuATSM on the other hand is readily effluxed from normoxic cells containing normal oxygen levels. Whereas under hypoxic conditions, CuATSM was shown to release bioavailable Cu likely due to selective Cu^{II}/Cu^{I} reduction at lower pH[33] and impairment of the mitochondrial electron transfer complex (ETC),[9,23] which results in the decrease in reoxidation and efflux of the Cu complex.

The presence and redox cycling of copper can be toxic to cells by multiple mechanisms. The released Cu(I) can activate hydrogen peroxide (H_2O_2) to generate hydroxide (OH^-) and hydroxyl radical (OH•) via Fenton reaction to produce reactive oxygen species (ROS).[34] However, CuL^{1-3} showed no significant ROS activity at concentrations of 1 – 10 μM (see Supplementary Information). Other mechanisms that may contribute include inactivation of proteasomal activity, topoisomerase inhibition, protein transmetalation, and damage to proteins, membranes, mitochondria, or DNA.[14,35-40] In a few cases, specific molecular targets of CuBTSCs or related complexes have been identified, including NPL4[41], FDX1 mitochondrial reductase[42] and more recently, a specific copper-mediated cell death mechanism known as "cuproptosis"—distinct from other forms of cell death such as apoptosis or ferroptosis.[43] In cuproptosis induced by copper (II) elesclomol (a BSTC-like bis(thiohydrazide) amide ionophore)[44] FDX1 mediates reduction of the

complex and release of Cu^{I}. Subsequent binding of Cu to lipoylated mitochondrial enzymes causes them to aggregate, triggering proteotoxic stress and cell death.[43]

The Cu(TSTC) complexes CuL^{1-3} in the current study have similar electronic structures, but different physical structures that result in different activity and selectivity. A survey of the antiproliferation activity and physical structures suggests the identity of the ligand backbone substituents and the orientation with respect to the various pendent groups influence activity and selectivity. Specifically, the presence of a small (Me, H) backbone substituent on the same side of the molecule as a TSC moiety (-NHMe) improves activity relative to CuL^3 in comparison with a bulkier (Ph) group on the TSC side. This is clearly demonstrated by the increased A549 activity of CuL^1 relative to its constitutional isomer CuL^2 and is also consistent with the higher A549 activities of CuL^3 and CuGTSM. However, complexes with a backbone H group show no selectivity between A549 and IMR-90 cells as observed for CuL^3 and CuGTSM. This may be due to decreased kinetic stability of the aldimine (RCH=NR) backbones in CuL^3 and CuGTSM complexes relative to the ketimine (R_2C=R) backbones in $CuL^{1,2}$. Overall, these results provide guiding principles for the further design of biologically active copper complexes.

Supporting Information

The following files are available free of charge: experimental details; crystallographic data and refinement parameters; NMR, FT-IR, UV-vis, EPR spectra, and ROS assays (PDF). CCDC 2194389−2194390 contain the supplementary crystallographic data for this paper. These data can be obtained free of charge via www.ccdc.cam.ac.uk/data_request/cif, or by emailing data_request@ccdc.cam.ac.uk, or by contacting The Cambridge Crystallographic Data Centre, 12 Union Road, Cambridge CB2 1EZ, UK; fax: +44 1223 336033.

Corresponding Author

Paula J. Bates email: paula.bates@louisville.edu, ORCID 0000-0002-4622-4152

Robert M. Buchanan email: robert.buchanan@louisville.edu, ORCID 0000-0001-8653-5388

Craig A. Grapperhaus, email: craig.grapperhaus@louisville.edu, ORCID 0000-0003-4889-2645

Other Authors

Kritika Bajaj, ORCID 0000-0001-8073-9320

Sarah A. Andres, ORCID 0000-0003-1751-8597

Dillon T. Hofsommer, ORCID 0000-0001-8638-2465

Aidan F. Greene, ORCID 0000-0002-8621-8371

Oleksandr Hietsoi, ORCID 0000-0003-0332-1064

Theresa Weis

Levi J. Beverly, ORCID 0000-0003-4652-4881

Mark S. Mashuta, ORCID 0000-0002-2724-7252

Author Contributions

The manuscript was written through contributions of all authors. All authors have given approval to the final version of the manuscript.

Funding Sources

This research was supported by the National Science Foundation CHE-1955268 (CAG) and CHE-1800245 (RMB) and the National Institutes of Health U01 HL127518 (PJB), which was funded by NIMHD, NHGRI, NHLBI, NIA, NIAAA, NIBIB, NICHD, NIDA, NINDS, NINR, and

NLN. The Department of Energy (DEFG02-08CH11538) and the Kentucky Research Challenge Trust Fund are acknowledged for upgrade of the X-ray facility (MSM).

Notes

The authors declare the following competing financial interest(s): Results described in this manuscript are included in an issued US patent (US-11208379-B2) entitled "Compounds, Compositions, Methods for Treating Diseases, and Methods for Preparing Compounds."

References

1. Krasnovskaya, O.; Naumov, A.; Guk, D.; Gorelkin, P.; Erofeev, A.; Beloglazkina, E.; Majouga, A. Copper Coordination Compounds as Biologically Active Agents. *Int. J. Mol. Sci.* **2020**, *21* (11), 3965. 10.3390/ijms21113965.

2. Que, E. L.; Domaille, D. W.; Chang, C. J. Metals in Neurobiology: Probing Their Chemistry and Biology with Molecular Imaging. *Chem. Rev.* **2008**, *108* (5), 1517-1549. 10.1021/cr078203u.

3. Solomon, E. I.; Sundaram, U. M.; Machonkin, T. E. Multicopper Oxidases and Oxygenases. *Chem. Rev.* **1996**, *96* (7), 2563-2606. 10.1021/cr950046o.

4. Ge, E. J.; Bush, A. I.; Casini, A.; Cobine, P. A.; Cross, J. R.; DeNicola, G. M.; Dou, Q. P.; Franz, K. J.; Gohil, V. M.; Gupta, S.; Kaler, S. G.; Lutsenko, S.; Mittal, V.; Petris, M. J.; Polishchuk, R.; Ralle, M.; Schilsky, M. L.; Tonks, N. K.; Vahdat, L. T.; Van Aelst, L.; Xi, D.; Yuan, P.; Brady, D. C.; Chang, C. J. Connecting copper and cancer: from transition metal signalling to metalloplasia. *Nat. Rev. Cancer* **2022**, *22* (2), 102-113. 10.1038/s41568-021-00417-2.

5. Brady, D. C.; Crowe, M. S.; Turski, M. L.; Hobbs, G. A.; Yao, X.; Chaikuad, A.; Knapp, S.; Xiao, K.; Campbell, S. L.; Thiele, D. J.; Counter, C. M. Copper is required for oncogenic BRAF signalling and tumorigenesis. *Nature* **2014**, *509* (7501), 492-496. 10.1038/nature13180.

6. Chang, C. J. Searching for harmony in transition-metal signaling. *Nat. Chem. Biol.* **2015**, *11* (10), 744-747. 10.1038/nchembio.1913.

7. McKenzie-Nickson, S.; Bush, A. I.; Barnham, K. J. Bis(thiosemicarbazone) Metal Complexes as Therapeutics for Neurodegenerative Diseases. *Curr. Top. Med. Chem.* **2016**, *16* (27), 3058-3068. 10.2174/1568026616666160216155746.

8. Nikseresht, S.; Hilton, J. B.; Kysenius, K.; Liddell, J. R.; Crouch, P. J. Copper-ATSM as a treatment for ALS: Support from mutant SOD1 models and beyond. *Life* **2020**, *10* (11), 271. 10.3390/life10110271.

9. Fujibayashi, Y.; Taniuchi, H.; Yonekura, Y.; Ohtani, H. Copper-62-ATSM: a new hypoxia imaging agent with high membrane permeability and low redox potential. *J. Nucl. Med.* **1997**, *38* (7), 1155.

10. Ikawa, M.; Okazawa, H.; Tsujikawa, T.; Matsunaga, A.; Yamamura, O.; Mori, T.; Hamano, T.; Kiyono, Y.; Nakamoto, Y.; Yoneda, M. Increased oxidative stress is related to disease severity in the ALS motor cortex: a PET study. *Neurology* **2015**, *84* (20), 2033-2039. 10.1212/WNL.0000000000001588.

11. Ikawa, M.; Okazawa, H.; Nakamoto, Y.; Yoneda, M. PET imaging for oxidative stress in neurodegenerative disorders associated with mitochondrial dysfunction. *Antioxidants* **2020**, *9* (9), 861. 10.3390/antiox9090861.

12. Palanimuthu, D.; Shinde, S. V.; Somasundaram, K.; Samuelson, A. G. In Vitro and in Vivo Anticancer Activity of Copper Bis(thiosemicarbazone) Complexes. *J. Med. Chem.* **2013**, *56* (3), 722-734. 10.1021/jm300938r.

13. Pelosi, G. Thiosemicarbazone Metal Complexes: From Structure to Activity. *Open Cryst. J.* **2010**, *3*, 16-28. 10.2174/1874846501003010016.

14. Dalecki, A. G.; Crawford, C. L.; Wolschendorf, F. Copper and Antibiotics: Discovery, Modes of Action, and Opportunities for Medicinal Applications. *Adv. Microb. Physiol.* **2017**, 193-260. 10.1016/bs.ampbs.2017.01.007.

15. Bajaj, K.; Buchanan, R. M.; Grapperhaus, C. A. Antifungal activity of thiosemicarbazones, bis(thiosemicarbazones), and their metal complexes. *J. Inorg. Biochem.* **2021**, *225*. 10.1016/j.jinorgbio.2021.111620.

16. Cater, M. A.; Pearson, H. B.; Wolyniec, K.; Klaver, P.; Bilandzic, M.; Paterson, B. M.; Bush, A. I.; Humbert, P. O.; La Fontaine, S.; Donnelly, P. S. Increasing intracellular bioavailable copper selectively targets prostate cancer cells. *ACS Chem. Biol.* **2013**, *8* (7), 1621-1631. 10.1021/cb400198p.

17. Palma, E.; Raposinho, P.; Campello, M. P. C.; Belo, D.; Guerreiro, J. F.; Alves, V.; Fonseca, A.; Abrunhosa, A. J.; Paulo, A.; Mendes, F. Anticancer Activity and Mode of Action of Copper(II)-Bis(thiosemicarbazonato) Complexes with Pendant Nitrogen Heterocycles. *Eur. J. Inorg. Chem.* **2021**, *2021* (14), 1337-1348. 10.1002/ejic.202100168.

18. Vishnosky, N. S.; Mashuta, M. S.; Buchanan, R. M.; Grapperhaus, C. A. Syntheses, structures, and electrochemical studies of N, N'-bis (alkylthiocarbamate) butane-2,3-diimine

Cu(II) complexes as pendent alkoxy derivatives of Cu(ATSM). *Inorg. Chim. Acta* **2017**, 45-51. 10.1016/j.ica.2017.02.003.

19. Andres, S. A.; Bajaj, K.; Vishnosky, N. S.; Peterson, M. A.; Mashuta, M. S.; Buchanan, R. M.; Bates, P. J.; Grapperhaus, C. A. Synthesis, Characterization, and Biological Activity of Hybrid Thiosemicarbazone–Alkylthiocarbamate Metal Complexes. *Inorg. Chem.* **2020**, *59* (7), 4924-4935. 10.1021/acs.inorgchem.0c00182.

20. Oliveri, V. Selective Targeting of Cancer Cells by Copper Ionophores: An Overview. *Front. Mol. Biosci.* **2022**, *9*. 10.3389/fmolb.2022.841814.

21. Maurer, R. I.; Blower, P. J.; Dilworth, J. R.; Reynolds, C. A.; Zheng, Y. F.; Mullen, G. E. D. Studies on the mechanism of hypoxic selectivity in copper bis(thiosemicarbazone) radiopharmaceuticals. *J. Med. Chem.* **2002**, *45* (7), 1420-1431. 10.1021/jm0104217.

22. Xiao, Z.; Donnelly, P. S.; Zimmermann, M.; Wedd, A. G. Transfer of copper between bis(thiosemicarbazone) ligands and intracellular copper-binding proteins. Insights into mechanisms of copper uptake and hypoxia selectivity. *Inorg. Chem.* **2008**, *47* (10), 4338-4347. 10.1021/ic702440e.

23. Donnelly, P. S.; Liddell, J. R.; Lim, S.; Paterson, B. M.; Cater, M. A.; Savva, M. S.; Mot, A. I.; James, J. L.; Trounce, I. A.; White, A. R.; Crouch, P. J. An impaired mitochondrial electron transport chain increases retention of the hypoxia imaging agent diacetylbis(4-methylthiosemicarbazonato)copper(II). *Proc. Natl. Acad. Sci. U. S. A.* **2012**, *109* (1), 47-52. 10.1073/pnas.1116227108.

24. John, E. K.; Green, M. A. Structure-activity relationships for metal-labeled blood flow tracers: comparison of keto aldehyde bis (thiosemicarbazonato) copper (II) derivatives. *J. Med. Chem.* **1990**, *33* (6), 1764-1770. 10.1021/jm00168a035.

25. Subczynski, W. K.; Antholine, W. E.; Hyde, J. S.; Petering, D. H. Orientation and mobility of a copper square-planar complex in a lipid bilayer. *J. Am. Chem. Soc.* **1987**, *109* (1), 46-52. 10.1021/ja00235a007.

26. Bajaj, K.; Andres, S. A.; Hofsommer, D. T.; Galib, M.; Mashuta, M. S.; Bennett, B.; Narayanan, B.; Buchanan, R. M.; Bates, P. J.; Grapperhaus, C. A. Investigations of Bis(alkylthiocarbamato)copper Linkage Isomers. *Inorg. Chem.* **2022**, *61* (20), 7715-7719. 10.1021/acs.inorgchem.2c00371.

27. Reüfenacht, K. Arbetien über Phosphosäure- und Thiosphosphorsäureester mit einem Heterocyclischen Substituenten Thiadiazol-Ringschluss und eine Dabei Auftretende Methylübertragung. *Helv. Chim. Acta* **1972**, *55*, 1178-1187. 10.1002/hlca.19720550414.

28. Xie, D.; King, T. L.; Banerjee, A.; Kohli, V.; Que, E. L. Exploiting Copper Redox for F-19 Magnetic Resonance-Based Detection of Cellular Hypoxia. *J. Am. Chem. Soc.* **2016**, *138* (9), 2937-2940. 10.1021/jacs.5b13215.

29. Sheldrick, G. M. A short history of SHELX. *Acta Crystallogr A* **2008**, *64* (1), 112-122. 10.1107/S0108767307043930.

30. Morgan, D. M. Tetrazolium (MTT) assay for cellular viability and activity. *Methods Mol. Biol.* **1998**, *79*, 179-183. 10.1385/0-89603-448-8:179.

31. Winkelmann, D. A.; Bermke, Y.; Petering, D. H. Comparative properties of the antineoplastic agent, 3-ethoxy-2-oxobutyraldehyde bis(thiosemicarbazonato) copper(II) and related chelates: Linear free energy correlations. *Bioinorg. Chem.* **1974**, *3* (3), 261-277. 10.1016/S0006-3061(00)80074-5.

32. Minkel, D. T.; Saryan, L. A.; Petering, D. H. Structure-Function Correlations in the Reaction of Bis(thiosemicarbazonato) Copper(II) Complexes with Ehrlich Ascites Tumor Cells1. *Cancer Res.* **1978**, *38* (1), 124-129.

33. Lopez, J.; Ramchandani, D.; Vahdat, L. Copper depletion as a therapeutic strategy in cancer. *Met. Ions Life Sci* **2019**, *19*, 303-330. 10.1515/9783110527872-018.

34. Gupta, P.; Lakes, A.; Dziubla, T. A free radical primer. In *Oxidative stress and biomaterials*, Elsevier, 2016; pp 1-33.

35. Denoyer, D.; Clatworthy, S. A.; Cater, M. A. Copper complexes in cancer therapy. *Met. Ions Life Sci* **2018**, *18*, 469-506. 10.1515/9783110470734-022.

36. Paterson, B. M.; Donnelly, P. S. Copper complexes of bis(thiosemicarbazones): from chemotherapeutics to diagnostic and therapeutic radiopharmaceuticals. *Chem. Soc. Rev.* **2011**, *40* (5), 3005-3018. 10.1039/c0cs00215a.

37. Santini, C.; Pellei, M.; Gandin, V.; Porchia, M.; Tisato, F.; Marzano, C. Advances in copper complexes as anticancer agents. *Chem. Rev.* **2014**, *114* (1), 815-862. 10.1021/cr400135x.

38. Santoro, A.; Vileno, B.; Palacios, Ò.; Peris-Díaz, M. D.; Riegel, G.; Gaiddon, C.; Krężel, A.; Faller, P. Reactivity of Cu (II)–, Zn (II)–and Fe (II)–thiosemicarbazone complexes with

glutathione and metallothionein: from stability to dissociation to transmetallation. *Metallomics* **2019**, *11* (5), 994-1004. 10.1039/c9mt00061e.

39. Wehbe, M.; Leung, A. W. Y.; Abrams, M. J.; Orvig, C.; Bally, M. B. A Perspective - can copper complexes be developed as a novel class of therapeutics? *Dalton Trans.* **2017**, (*33*), 10758-10773. 10.1039/c7dt01955f.

40. Zaltariov, M. F.; Hammerstad, M.; Arabshahi, H. J.; Jovanovic, K.; Richter, K. W.; Cazacu, M.; Shova, S.; Balan, M.; Andersen, N. H.; Radulović, S. a. New iminodiacetate–thiosemicarbazone hybrids and their copper (II) complexes are potential ribonucleotide reductase R2 inhibitors with high antiproliferative activity. *Inorg. Chem.* **2017**, *56* (6), 3532-3549. 10.1021/acs.inorgchem.6b03178.

41. Skrott, Z.; Mistrik, M.; Andersen, K. K.; Friis, S.; Majera, D.; Gursky, J.; Ozdian, T.; Bartkova, J.; Turi, Z.; Moudry, P. Alcohol-abuse drug disulfiram targets cancer via p97 segregase adaptor NPL4. *Nature* **2017**, *552* (7684), 194-199. 10.1038/nature25016.

42. Tsvetkov, P.; Detappe, A.; Cai, K.; Keys, H. R.; Brune, Z.; Ying, W.; Thiru, P.; Reidy, M.; Kugener, G.; Rossen, J. Mitochondrial metabolism promotes adaptation to proteotoxic stress. *Nat. Chem. Biol.* **2019**, *15* (7), 681-689. 10.1038/s41589-019-0291-9.

43. Tsvetkov, P.; Coy, S.; Petrova, B.; Dreishpoon, M.; Verma, A.; Abdusamad, M.; Rossen, J.; Joesch-Cohen, L.; Humeidi, R.; Spangler, R. D. Copper induces cell death by targeting lipoylated TCA cycle proteins. *Science* **2022**, *375* (6586), 1254-1261. 10.1126/science.abf052.

44. O'Day, S. J.; Eggermont, A. M.; Chiarion-Sileni, V.; Kefford, R.; Grob, J. J.; Mortier, L.; Robert, C.; Schachter, J.; Testori, A.; Mackiewicz, J. Final results of phase III SYMMETRY study:

randomized, double-blind trial of elesclomol plus paclitaxel versus paclitaxel alone as treatment for chemotherapy-naive patients with advanced melanoma. *J. Clin. Oncol.* **2013**, *31* (9), 1211-1218. 10.1200/JCO.2012.44.5585.

TOC

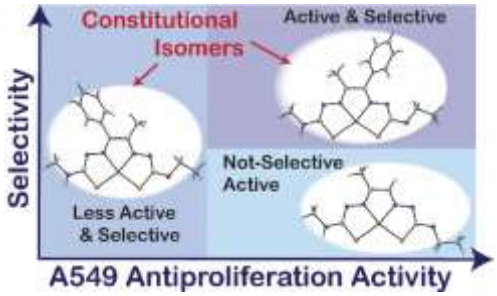
Constitutional
Isomers
Active & Selective
Selectivity
Not-Selective
Active
Less Active
& Selective
A549 Antiproliferation Activity